PHYSICAL REVIEW B **95**, 144402 (2017)

Spin superfluid Josephson quantum devices

So Takei,[1,2] Yaroslav Tserkovnyak,[3] and Masoud Mohseni[4]
[1]*Department of Physics, Queens College of the City University of New York, Queens, New York 11367, USA*
[2]*The Graduate Center of the City University of New York, New York, New York 10016, USA*
[3]*Department of Physics and Astronomy, University of California, Los Angeles, Los Angeles, California 90095, USA*
[4]*Google Inc, Venice, California 90291, USA*

(Received 23 July 2016; revised manuscript received 11 March 2017; published 4 April 2017)

A macroscopic spintronic qubit based on spin superfluidity and spin Hall phenomena is proposed. This magnetic quantum information processing device realizes the spin-supercurrent analog of the superconducting phase qubit and allows for full electrical control and readout. We also show that an array of interacting magnetic phase qubits can realize a quantum annealer. These devices can be built through standard solid-state fabrication technology, allowing for scalability. However, the upper bound for the operational temperature can, in principle, be higher than the superconducting counterpart, as it is ultimately governed by the magnetic ordering temperatures, which could be much higher than the critical temperatures of the conventional superconducting devices.

DOI: 10.1103/PhysRevB.95.144402

I. INTRODUCTION

Macroscopic quantum phenomena in magnetic systems has been a topic of active research for a number of years. Manifestations of such phenomena have been discussed in the context of ferromagnetic domain walls [1], magnetic nanoparticles [2,3], as well as molecular magnets [4]. Molecular magnets, in particular, have garnered much attention for their potential utility in quantum information technology [5]. Despite these activities, research addressing the possibility of macroscopic qubits in magnetic systems still remains essentially absent. In this work, we propose the first macroscopic spin-based qubit by combining two recent advancements in the field of spintronics: spin superfluidity and spin Hall phenomena.

Spin superfluidity explores how analogs of conventional superfluidity can be realized in magnetically ordered systems [6]. The Josephson effect in conventional superfluids involves a dissipationless mass flow between two weakly coupled superfluids and relies on macroscopic phase coherence of the superfluids, each characterized by a U(1) order parameter. Magnetic order in certain insulating magnets is also described by macroscopic U(1) order parameters [6]. In analogy with conventional superfluidity, coupling two such magnets gives rise to the *magnetic* Josephson effect involving dissipationless (superfluid) flow of spin angular momentum between the magnets [7]. Spin Hall phenomenology is often discussed in the context of a bilayer system consisting of a normal metal with strong spin-orbit coupling and an insulating ferromagnet [8]. The combination of spin-orbit coupling in the metal and exchange coupling (between the conduction electron spins and the magnetic moments in the insulator) at the metal|magnet interface allows angular momentum to be transferred from the metal's crystal lattice to the ferromagnet, thus engendering macroscopic coupling between the electrical current in the metal and the magnetic order parameter [9].

In this work, we show that a heterostructure consisting of magnetic insulators and a normal metal with strong spin-orbit coupling realizes a magnetic analog of the superconducting phase qubit [10] and permits full electrical control and readout via spin Hall phenomena (see Fig. 1). We refer to this device as the *magnetic phase qubit*. While electrical readout of molecular qubits can be challenging [5], spin Hall phenomena offers an alternative, and a possibly more straightforward method for electrical control and readout of the magnetic qubit. The device is an example of a macroscopic qubit that can be constructed from solid-state materials and so should offer the same advantages as the superconducting qubits of strong interqubit coupling and scalability. The magnetic qubit is based on antiferromagnets, which are known to display macroscopic quantum behavior at higher temperatures than ferromagnets [2]. We estimate the operational temperature of the qubit to be $T \approx 3$ K, which, in contrast to superconducting qubits, can be achieved by a pure helium-4 cryostat without a dilution fridge. Furthermore, the zero net magnetization in antiferromagnets implies that they do not generate stray fields; this is advantageous when coupling qubits, as it will eliminate any unwanted magnetic crosstalk between neighboring qubits. We find that the relaxation time scale for our qubit is relatively small, with $T_1 \approx 10$ ns, because it is set in our device by the internal magnetic dynamics of the antiferromagnet (known to be in the terahertz range) [11]. Finally, we show that a coupled array of these qubits can realize a quantum annealer [12], which could be used to solve certain optimization problems.

II. MODEL AND THEORY

The prototype magnetic phase qubit consists of an isotropic (Heisenberg) antiferromagnetic insulator (AF) attached to a normal metal (N) with strong spin-orbit coupling, exchange coupled to a fixed ferromagnetic layer, and subjected to an external magnetic field in the $-z$ direction (see Fig. 1). We consider low enough temperatures such that only the lowest mode is excited in the AF and it can be considered in the mono-domain limit (upper bound on temperature for mono-domain operation is estimated in Sec. VI). A bipartite AF can be characterized by two variables, $\boldsymbol{n}(t)$ and $\boldsymbol{M}(t)$, representing the Néel vector and the total spin angular momentum in the AF, respectively [13]. These variables are chosen to satisfy $|\boldsymbol{n}| = 1$ and $\boldsymbol{n} \cdot \boldsymbol{M} = 0$, the presence of strong Néel order implying $|\boldsymbol{M}|/S \ll 1$ (S being twice the total spin angular momentum on one sublattice in units of $\hbar$). The AF Lagrangian and its coupling to the ferromagnet can then be written as $L = \hbar \boldsymbol{n} \cdot$

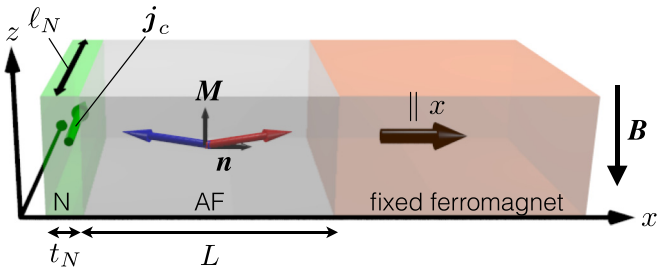

FIG. 1. The magnetic phase qubit. A mono-domain antiferromagnet (AF) is exchange coupled to a fixed mono-domain ferromagnet (with its macrospin oriented along the x axis) and attached to a normal metal (N) with strong spin-orbit coupling. Charge current j_c is applied in the y direction in the N. Here, $\boldsymbol{M}$ denotes the total spin angular momentum in the AF, while $\boldsymbol{n}$ denotes the unit vector parallel to the Néel order.

$(\boldsymbol{M}\times\boldsymbol{n})-\boldsymbol{M}^2/2\chi+bM_z+Jn_x$, where $b=\hbar\gamma_0|\boldsymbol{B}|$ (with γ_0 the gyromagnetic ratio and $\boldsymbol{B}$ the magnetic field), J is the AF-ferromagnet exchange coupling, and χ is the AF spin susceptibility. The N is taken to be a metal with strong spin-orbit coupling [e.g., platinum (Pt)], and is assumed to be a metallic film parallel to the yz plane obeying Ohm's law $\rho\boldsymbol{j}_c=\boldsymbol{E}$, where $\boldsymbol{E}$ is the electric field, $\boldsymbol{j}_c$ is the linear charge current density, and ρ is its two-dimensional (2D) resistivity.

The current in the N can be used to manipulate the spins in the AF. This is achieved by a combination of spin-orbit coupling in the N and the exchange coupling at the N|AF interface, which allows angular momentum to be transferred from the N crystal lattice to the AF spins, effectively generating a macroscopic coupling between the current and the AF variables $\boldsymbol{n}$ and $\boldsymbol{M}$ [14]. Through this magnetoelectric coupling, the current generates torques on the AF spins, thus resulting in an injection of spin current $\boldsymbol{j}_s$ into the AF, and the AF dynamics, in turn, induces an electromotive force $\boldsymbol{\varepsilon}$ in the N. Spin Hall phenomenology allows one to write down general expressions for $\boldsymbol{\varepsilon}$ and $\boldsymbol{j}_s$ that respect certain crystalline and structural symmetries at the interface [15]. In the presence of full translational and rotational symmetries in the yz plane and the breaking of reflection symmetry along the x axis, $\boldsymbol{\varepsilon}$ within spin Hall phenomenology reads

$$\boldsymbol{\varepsilon}=\vartheta(\boldsymbol{n}\times\dot{\boldsymbol{n}})\times\hat{\boldsymbol{x}}\,, \tag{1}$$

and the spin current entering the AF takes the form

$$\boldsymbol{j}_s=\mathscr{A}\vartheta\boldsymbol{n}\times(\hat{\boldsymbol{x}}\times\boldsymbol{j}_c)\times\boldsymbol{n}\,. \tag{2}$$

Here, $\mathscr{A}$ is the cross-sectional area of the interface and ϑ is a phenomenological torque coefficient for the N|AF interface. The fact that the same coefficient ϑ enters both Eqs. (1) and (2) is a consequence of Onsager reciprocity [8]. In Eq. (1), we have ignored the so-called reactive contribution $\propto\dot{\boldsymbol{n}}\times\hat{\boldsymbol{x}}$ (also allowed by symmetry), as it typically gives a significantly smaller contribution compared to the term in Eq. (1) for diffusive metals like the N considered here [15]. Equation (1) was obtained under the assumption that the AF Néel order is collinear; this is a good approximation as long as all energy scales are small with respect to the AF exchange scale.

The analysis of the AF dynamics here follows Ref. [13] very closely. For $\boldsymbol{j}_c=0$, $\boldsymbol{n}$ lies in the xy plane and the field gives a finite total spin $\boldsymbol{M}=\chi b\hat{\boldsymbol{z}}$. For a nonzero $\boldsymbol{j}_c=j_c\hat{\boldsymbol{y}}$, the AF dynamics can be described in terms of a dynamic Néel vector confined within the xy plane, i.e., $\boldsymbol{n}=[\cos\varphi(t),\sin\varphi(t),0]$, and an additional canting $\xi(t)$ defined via $\boldsymbol{M}(t)=[\chi b+\xi(t)]\hat{\boldsymbol{z}}$. Linearizing the AF dynamics in $\xi(t)$ and $\dot{\varphi}(t)$ and phenomenologically introducing viscous magnetic damping in the AF, the coupled dynamics of the current and the AF variables become [13]

$$\hbar\dot{\varphi}=\frac{\xi}{\chi}+\frac{\hbar\alpha'}{S}\dot{\xi}\,,\qquad \hbar\dot{\xi}=-J\sin\varphi+j-\hbar\alpha S\dot{\varphi}\,, \tag{3}$$

and $\rho\boldsymbol{j}_c=\boldsymbol{E}+\boldsymbol{\varepsilon}$, where $j\equiv\mathscr{A}\vartheta j_c$, and α, α' are two independent Gilbert damping parameters. The N subjects the AF to additional viscous damping, which modifies the spin current term in Eq. (2) to $\boldsymbol{j}_s\to\boldsymbol{j}_s'\equiv\boldsymbol{j}_s-\hbar\alpha^{\uparrow\downarrow}S\boldsymbol{n}\times\dot{\boldsymbol{n}}$. If N is a perfect spin sink (as for Pt), $\alpha^{\uparrow\downarrow}=\mathscr{A}g^{\uparrow\downarrow}/4\pi S$, where $g^{\uparrow\downarrow}$ is the (real part of the) effective interfacial spin-mixing conductance per unit area. This shifts $\alpha\to\tilde{\alpha}=\alpha+\alpha^{\uparrow\downarrow}$ and $\alpha'\to\tilde{\alpha}'$ in Eq. (3). (The precise expression for $\tilde{\alpha}'$ is unimportant here since it will not play a crucial role in the following discussion.) As Eq. (3) neglects the mode corresponding to the Néel vector oscillating out of the xy plane (with a gap of b), it is an appropriate description of the AF dynamics as long as $b>\sqrt{J/\chi}$.

For $\tilde{\alpha}=\tilde{\alpha}'=0$, noticing that ξ is the momentum conjugate to φ, the effective Hamiltonian corresponding to Eq. (3) is given by ($\eta\equiv j/J$)

$$H_{\rm eff}=\frac{\xi^2}{2\chi}-J(\cos\varphi+\eta\varphi)\equiv\frac{\xi^2}{2\chi}+U(\varphi)\,. \tag{4}$$

Well below the Néel temperature, $\chi\sim N/J_{\rm AF}$, where N is the total number of spins in the AF and $J_{\rm AF}$ is its internal AF exchange scale. Since $N\gg1$, it is reasonable to assume the regime $J\chi\gg1$. Then the Josephson term (proportional to J) dominates in $H_{\rm eff}$, which then has the same form as the standard current-biased Josephson junction with the charging energy given by χ^{-1} and the Josephson energy by the exchange coupling J. Here, the "bias current" j is a flow of (z-polarized) spin across the N|AF interface and is fully controllable using the external *charge* current j_c. Interestingly, while the torque in Eq. (2) [which gives rise to the term proportional to η in Eq. (4)] is dissipative in the sense that it is odd under time reversal, its effects enter the AF dynamics in a way still accountable by purely Hamiltonian dynamics.

III. DEFINING THE QUBIT

The following results closely follow those for the superconducting phase qubits [16,17]. We emphasize that the qubit is operated at $\eta\lesssim1$ to ensure only a few states are present in a washboard potential minimum. In this regime, the potential about $\varphi=\pi/2$ can be approximated by a cubic form $U(\phi)\approx(J-j)\phi-J\phi^3/6+\text{const.}$ (with $\phi\equiv\varphi-\pi/2$). A local minimum is located at $\phi_0=-\sqrt{2(1-\eta)}$, and the oscillation frequency corresponding to the quadratic curvature at the minimum is given by

$$\hbar\omega_p=\sqrt{J/\chi}[2(1-\eta)]^{1/4}.$$

Imposing the canonical commutation relation $[\hat{\varphi},\hat{\xi}]=i$ leads to the quantization of energy levels inside the cubic potential,

and when $\eta \lesssim 1$ only a few quantum states are bound in each of the local minima. We label the lowest three energy eigenvalues by E_0, E_1, and E_2, and the corresponding states by $|0\rangle$, $|1\rangle$, and $|2\rangle$. Taking account of the cubic anharmonicity to second order in perturbation theory, the separation between the two lowest pairs of energy levels becomes $E_1 - E_0 \equiv \hbar\omega_{10} \approx \hbar\omega_p(1-r)$ and $E_2 - E_1 \equiv \hbar\omega_{21} \approx \hbar\omega_p(1-2r)$, where the deviations from the harmonic limit are quantified in terms of $r \equiv (5/36)(\hbar\omega_p/\Delta U)$, $\Delta U \equiv J(4\sqrt{2}/3)(1-\eta)^{3/2}$ being the energy barrier for the particle to escape from a local minimum.

A. Qubit control

The state of the qubit can be controlled by introducing an ac component to j oscillating at frequency ω_{10} [$j(t) = j_{\rm dc} + j_{\rm ac}(t)\cos(\omega_{10}t)$], where $j_{\rm dc}$ is the dc component and $j_{\rm ac}(t)$ modulates the amplitude of the ac component. The ac component to j can be introduced simply by adding an ac component to the charge current. To inhibit transitions between states $|1\rangle$ and $|2\rangle$, one requires the temporal variations of $j_{\rm ac}(t)$ to be slow compared to $2\pi/(\omega_{21} - \omega_{10})$. In this limit, and for temperatures $T \ll \hbar\omega_{10}/k_B$, the Hilbert space for the qubit is spanned by the two lowest states $|0\rangle$ and $|1\rangle$, and the effective Hamiltonian reads

$$\hat{H}_{\rm eff} = -\frac{\hbar\omega_{10}}{2}\hat{\sigma}^z - \frac{j_{\rm ac}(t)\gamma}{2}\begin{pmatrix} 0 & e^{i\omega_{10}t} \\ e^{-i\omega_{10}t} & 0 \end{pmatrix}, \qquad (5)$$

where $\gamma \equiv \sqrt{1/2\chi\hbar\omega_{10}}$, and we have invoked the rotating wave approximation and the off-diagonal elements were computed using harmonic oscillator states due to the small nonlinearity of the system. The qubit can undergo Rabi oscillations, where the probability for transition between $|0\rangle$ and $|1\rangle$ states $P_{0\to1}(t) = \sin^2[\Omega_{\rm ac}(t)t]$, where $\hbar\Omega_{\rm ac}(t) \equiv j_{\rm ac}(t)\gamma/2$. The application of an ac pulse over time interval $\Delta t = \pi/2\Omega_{\rm ac} \equiv t_0$ drives the qubit from state $|0\rangle$ to $|1\rangle$. With a pulse of length $\Delta t = t_0/2$, the qubit can be manipulated into the superposition state $(|0\rangle + |1\rangle)/\sqrt{2}$.

B. Qubit readout

The state of the qubit can be read out by adiabatically lowering the potential barrier ΔU close to E_1 such that the qubit in state $|1\rangle$ is (exponentially) more likely to tunnel out of a local minimum than that in state $|0\rangle$. The limit $\Delta U \to E_1$ is achieved as $\eta \to 1$ (see Sec. VI for further details). Once the "particle" tunnels out of the local minimum, it will descend down the washboard potential generating a finite $\langle\dot{\varphi}\rangle$, which induces an electromotive force $\boldsymbol{\varepsilon} \approx \vartheta\langle\dot{\varphi}\rangle\hat{\mathbf{y}}$, so that Ohm's law in the N is modified to $(\rho - \delta\rho)j_c = E$. Here, we neglect the z component of $\boldsymbol{\varepsilon}$ as it is counteracted by an electrostatic buildup along the z axis as long as the magnetic dynamics are slow compared to the relevant RC time of the normal metal. We can estimate $\delta\rho$ by considering the motion of the particle classically. Approximating the washboard potential as a downward-sloping line connecting all of the local minima, the descending particle (damped by Gilbert damping $\tilde{\alpha}$) will reach a terminal velocity $\dot{\varphi}_t = \mathscr{A}\vartheta j_c/\hbar\tilde{\alpha}S$. The correction to the effective resistivity thus reads $\delta\rho = \mathscr{A}\vartheta^2/\hbar\tilde{\alpha}S$. For a fixed j_c, $\delta\rho$ gives rise to a decrease in voltage of $\delta V = \delta\rho j_c \ell_N$ across the N, where ℓ_N is the length of the N in the y direction. The tunneling out of state $|1\rangle$ can be detected by detecting this voltage decrease. To detect state $|0\rangle$, one may transfer the qubit to state $|1\rangle$ using a resonant ac pulse, and then detect state $|1\rangle$.

IV. DECOHERENCE

A. Decoherence due to Gilbert damping

Decoherence in the magnetic phase qubit arises from various environmental degrees of freedom that couple to the macrospin, e.g., the phonons in the AF as well as the electron continuum in the N. Dissipation due to these environments has been accounted for by Gilbert damping. A damped macrospin experiences a stochastic force required to exist by the fluctuation-dissipation theorem [18]. The stochastic force can be described by introducing a random component $\delta H_{\rm eff}(t) = h_\varphi(t)\varphi + h_\xi(t)\xi$ to $H_{\rm eff}$, where $h_\varphi(t)$ and $h_\xi(t)$ are the stochastic fields. These stochastic fields modify Eq. (3) to

$$\hbar\dot{\xi} = -J\sin\varphi + j - \hbar\tilde{\alpha}S\dot{\varphi} - h_\varphi,$$
$$\hbar\dot{\varphi} = \frac{\xi}{\chi} + \frac{\hbar\tilde{\alpha}'}{S}\dot{\xi} + h_\xi.$$

Accounting for both thermal and quantum fluctuations, the correlation functions for the stochastic fields can be written as [17,18]

$$\langle h_\varphi(t)h_\varphi(0)\rangle = \int \frac{d\omega}{2\pi}\,\chi_\varphi(\omega)e^{-i\omega t},$$
$$\langle h_\xi(t)h_\xi(0)\rangle = \int \frac{d\omega}{2\pi}\,\chi_\xi(\omega)e^{-i\omega t},$$

where $\chi_\varphi(\omega) = \hbar^2\tilde{\alpha}\omega S\coth(\hbar\omega/2k_BT)$ and $\chi_\xi(\omega) = (\hbar^2\tilde{\alpha}'\omega/S)\coth(\hbar\omega/2k_BT)$. We now promote both φ and ξ to quantum-mechanical operators and project $\delta H_{\rm eff}(t)$ to the two lowest quantum states $|0\rangle$ and $|1\rangle$. If the states are again approximated as harmonic oscillator states, we have

$$\langle 0|\hat{\varphi}|1\rangle \approx \gamma, \quad \langle 0|\hat{\xi}|1\rangle \approx (2i\gamma)^{-1},$$

and the diagonal elements vanish. The stochastic contribution to the two-level Hamiltonian then becomes $\delta\hat{H}_{\rm eff}(t) = \tilde{h}_x(t)\hat{\sigma}^x + \tilde{h}_y(t)\hat{\sigma}^y$, with $\tilde{h}_x(t) = \gamma h_\varphi(t)$ and $\tilde{h}_y(t) = (2\gamma)^{-1}h_\xi(t)$. Here, the frequency spectra of the new noise fields obey $\tilde{\chi}_x(\omega) = \gamma^2\chi_\varphi(\omega)$ and $\tilde{\chi}_y(\omega) = (\tilde{\alpha}'/\tilde{\alpha})(2\gamma^2 S)^{-2}\chi_\varphi(\omega)$.

To estimate the T_1 and T_2 times, we consider the undriven qubit, i.e., $j_{\rm ac}(t) = 0$. We have $2\gamma^2 S \approx N(J\chi)^{-1/2} \gg 1$, so we may ignore the fluctuations $\tilde{h}_y(t)$ in this estimate. The relevant two-level Hamiltonian then reads

$$\hat{H}_{\rm eff} \approx -\frac{\hbar\omega_{10}}{2}\hat{\sigma}_z + \tilde{h}_x(t)\hat{\sigma}_x.$$

The noise term causes transitions between the two qubit states. If the qubit starts in state $|1\rangle$ at $t = 0$, the amplitude for the qubit to be in the ground state $|0\rangle$ at time t is given through Fermi's golden rule by

$$c_0(t) \approx \frac{1}{i\hbar}\int_0^t dt'\langle 0|\tilde{h}_x(t)\hat{\sigma}_x|1\rangle e^{i\omega_{10}t'}.$$

Similarly, if the qubit starts in state $|0\rangle$ at $t = 0$, the amplitude for the qubit to be in the excited state $|1\rangle$ at time t is given by

$$c_1(t) \approx \frac{1}{i\hbar}\int_0^t dt' \langle 1|\tilde{h}_x(t)\hat{\sigma}_x|0\rangle e^{-i\omega_{10}t'} .$$

The longitudinal relaxation rate is given by

$$\Gamma_1 = \dot{p}_0(t) + \dot{p}_1(t) ,$$

where $p_0(t) \equiv \langle |c_0(t)|^2\rangle$ and $p_1(t) \equiv \langle |c_1(t)|^2\rangle$. We find

$$p_0(t) + p_1(t) = \frac{2\gamma^2}{\hbar^2}\int \frac{d\omega}{2\pi}\frac{\sin^2\left(\frac{\omega-\omega_{10}}{2}t\right)}{\left(\frac{\omega-\omega_{10}}{2}\right)^2}\chi_\varphi(\omega) . \quad (6)$$

Most of the integral contribution in Eq. (6) comes from $\omega \approx \omega_{10}$, where $\chi(\omega)$ is a slowly varying function of ω but its prefactor inside the integrand is strongly peaked. Then the integral can be approximated by evaluating $\chi_\varphi(\omega)$ at $\omega = \omega_{10}$ and taking it out of the integral. This then leads to

$$\Gamma_1 \approx \frac{2\gamma^2\chi_\varphi(\omega_{10})}{\hbar^2} = \frac{\tilde{\alpha}S}{\chi\hbar} ,$$

where the result holds in the low-temperature regime, $k_BT \ll \hbar\omega_{10}$. Since the stochastic fields only involve transverse components, $\Gamma_2 = \Gamma_1/2$.

B. Decoherence due to fluctuating qubit splitting

Since the qubit splitting $\hbar\omega_{10}$ depends on the electrical current in the N, noise in the current can lead to a fluctuating qubit splitting and decoherence. Here, we consider this decoherence due to fluctuations in the dc component of the charge current j_c and for $j_{ac} = 0$. In the presence of the fluctuations, the effective two-level Hamiltonian Eq. (5) is endowed by a stochastic contribution given by

$$\hat{H}_0(t) = -\frac{\hbar\omega_{10}}{2}\hat{\sigma}_z - \frac{\hbar}{2L}\frac{\partial\omega_{10}}{\partial j_c}\delta I_c(t)\hat{\sigma}_z .$$

Here, $\delta I_c(t)$ is the noise in the dc charge current driven through the N and L is the thickness of the device in Fig. 1 along the z direction. Defining the symmetrized noise correlators for the stochastic fields as

$$\langle \delta I_c(t)\delta I_c(0)\rangle = \int \frac{d\omega}{2\pi} S_I(\omega)e^{-i\omega t}$$

and using standard results for noise and decoherence in quantum two-level systems, charge current noise gives rise to pure dephasing rate of

$$\Gamma_\varphi = \frac{1}{4L^2}\left(\frac{\partial\omega_{10}}{\partial j_c}\right)^2 S_I(0) . \quad (7)$$

V. QUBIT COUPLING

One may consider coupling many magnetic phase qubits in an array as shown in Fig. 2. Every qubit is coupled to its own N so that its splitting $\hbar\omega_{10,i}$ and the Rabi frequency $\Omega_{ac,i}$ can be tuned independently by adjusting the dc and ac amplitudes of $\boldsymbol{j}_{c,i}(t)$, respectively (i here labels the qubits). We connect neighboring AFs via a metallic "bridge" (shaded in blue) that gives rise to an effective exchange interaction J'_{ij} between the

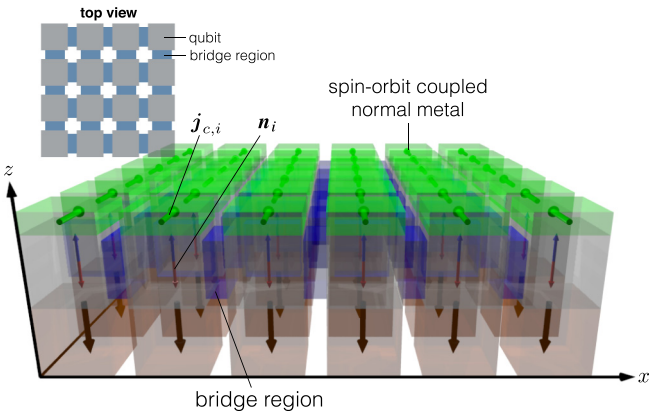

FIG. 2. A coupled array of magnetic phase qubits. Each qubit is coupled to its own normal metal with independently tunable dc and ac currents. The ferromagnetic region (shaded in blue) mediates a coupling between nearest-neighbor AFs and gives rise to interqubit coupling.

ith and jth Néel vectors. This coupling may be generated if the AFs expose more spins from one sublattice than the other to the metallic link, and if the conduction electrons in the metallic link (with thickness d) mediate a Ruderman-Kittel-Kasuya-Yosida (RKKY) interaction between these net spin moments. The RKKY interaction is generally an effective exchange interaction between two spin moments mediated by the conduction electrons in the metallic link. Using a standard result, the effective RKKY coupling (for $k_Fd \gg 1$) is $\propto J_0^2\cos(k_Fd)/(k_Fd)^3$, where k_F is the Fermi wave vector of the metallic spacer and J_0 is the interfacial exchange coupling between the spin densities in the link and the AF [19]. Therefore, electrostatic gating of each individual metallic spacer allows one to control the electron density (and thus k_F) of each spacer individually and allow local dynamic control of both the sign and the magnitude of J'_{ij}.

This coupling between the neighboring AFs gives rise to the interaction of the form $H_{int} = -\sum_{\langle i<j\rangle} J'_{ij}\cos(\varphi_i - \varphi_j)$, where $\langle i, j\rangle$ labels the nearest-neighbor qubits. Quantizing this Hamiltonian and projecting it to the two logical states of each qubit, the interaction Hamiltonian reads

$$\hat{H}_{int} = \frac{1}{4}\sum_{\langle i<j\rangle} J'_{ij}\gamma^2\hat{\sigma}_i^x\hat{\sigma}_j^x . \quad (8)$$

Here, we have neglected terms of order J'/J that only renormalize the qubit frequency ω_{10}. The coupled array of qubits is then described by the total Hamiltonian $\hat{H}_t = \hat{H}_0 + \hat{H}_{int}$, where

$$\hat{H}_0 = -\sum_i\left[\frac{\hbar\omega_{10,i}}{2}\hat{\sigma}_i^z + \frac{j_{ac,i}\gamma}{2}\begin{pmatrix}0 & \\ e^{i\omega_{10,i}t}e^{-i\omega_{10,i}t} & 0\end{pmatrix}\right] .$$

The coupled array of magnetic phase qubits as shown in Fig. 2 can be used to realize a quantum annealer. A quantum annealer solves hard optimization problems by finding the ground state of a "problem Hamiltonian" through a process involving quantum fluctuations. It can be implemented with a classical Ising Hamiltonian that encodes the computational problem, and a transverse field term, $\hat{H}_{QA}(t) = -A(t)\sum_i\hat{\sigma}_i^x + B(t)\hat{H}_{Ising}$,

where $\hat{H}_{\rm Ising} = -\sum_i h_i \hat{\sigma}_i^z - \sum_{i<j} J_{ij}\hat{\sigma}_i^z\hat{\sigma}_j^z$, i,j label lattice sites, and t runs from 0 to t_f. At $t = 0$ and temperature T, the quantum annealing process begins in the limit of strong transverse field, i.e., $A(0) \gg \{k_B T, |B(0)h_i|, |B(0)J_{ij}|\}\ \ \forall i,j$, when the quantum-mechanical fluctuations dominate, and then one gradually decreases $A(t)$ and increases $B(t)$ such that the state of the system approaches a classical bit string that ideally represents the ground state of the problem Hamiltonian. Generally, at sufficiently low temperatures, the quality of solution is improved when the time scale of the annealing schedule is substantially larger than the inverse of the square of the minimum gap between the instantaneous ground state and the first existing state of the effective many-body Hamiltonian given by $\hat{H}_{\rm QA}$. Rotating the spin axes of all the qubits by $\pi/2$ about the y axis (such that $\hat{\sigma}_{z,x} \to \pm\hat{\sigma}_{x,z}$), $\hat{H}_t$ can be shown to mimic the Hamiltonian $\hat{H}_{\rm QA}$ so the coupled array of magnetic phase qubits above can be used to implement quantum annealing.

VI. DISCUSSION

The qubit must operate at temperatures $k_B T \ll \hbar\omega_{10} \equiv k_B T_+ \approx \sqrt{J\chi^{-1}}$. A good candidate material for a Heisenberg AF is a cubic perovskite $KNiF_3$ [20], a spin-1 AF with $J_{\rm AF} \approx 0.01$ eV, and lattice constant of $a \approx 4$ Å. Let us consider a cube-shaped $KNiF_3$ with side length $L = 50$ nm. Assuming that the exchange coupling between the AF and the ferromagnet arises from the exchange bias effect with a corresponding field of $B_{\rm ex} \approx 100$ mT [21], we may take $J \approx \hbar\gamma B_{\rm ex}(L/a)^3$. Since $\chi \approx (L/a)^3/J_{\rm AF}$, we obtain $T_+ \approx 3$ K. Using $\alpha \approx 10^{-5}$ and assuming that the damping enhancement $\alpha^{\uparrow\downarrow}$ due to the N just exceeds α, we take $\tilde{\alpha} \approx 10^{-5}$ and we obtain $T_1 \approx 10$ ns. The nonlinearity necessary for the qubit to remain within the two-level subspace requires $\eta \approx 1$. The (linear) current density necessary to achieve this is $\bar{j}_c \approx J/\mathscr{A}\vartheta$. Here, $\vartheta = \hbar \tan\theta_{\rm SH}/2et_N$, where $\theta_{\rm SH}$ is the effective spin Hall angle for the N|AF interface and t_N is the N thickness [15]. Using $\theta_{\rm SH} \approx 0.1$ (appropriate for a Pt contact), $t_N = 10$ nm, and setting all other parameters to the values above, we obtain $\bar{j}_c \approx 3 \times 10^5$ A m^{-1}. Based on the same parameters and using $j_c \approx \bar{j}_c$, we obtain $\delta V \approx 100$ mV. Finally, from Eq. (8), we have $\tau_{2q}/T_1 \approx \tilde{\alpha}\hbar\omega_{10}/J'_{ij}$, where τ_{2q} is the two-qubit time scale. If we assume $J'_{ij} \approx J$, we obtain $\tau_{2q}/T_1 \approx 10^{-4}$. With $T_+ \approx 3$ K, the neglect of the out-of-plane Néel vector oscillations [see discussion following Eq. (3)] is justified as long as the external field $B > 2$ T.

Qubit readout is achieved by bringing $\Delta U \to \hbar\omega_{10}$, which translates to $1 - \eta \approx 10^{-4}$ (using $B_{\rm ex} \approx 100$ mT, $J_{\rm AF}/k_B \approx 100$ K, and $L/a \approx 125$) and $\Delta U \approx 10^{-5} J$. Recall that $\Delta U \propto (1-\eta)^{5/4}$ and $\hbar\omega_{10} \propto (1-\eta)^{1/4}$. The difference in the exponents gives a separation of energy scales between the two variables so that, as $\eta \to 1$, the barrier ΔU can be lowered while keeping the qubit levels well separated. Indeed, even for $1 - \eta \approx 10^{-4}$, $\hbar\omega_{10}$ remains of the order $\sqrt{J/\chi}$.

We now estimate the dephasing rate Eq. (7). Using $1 - \eta \approx 10^{-4}$ (together with the other parameters given above), we find

$$\Gamma_\varphi \approx (2.3 \times 10^{31}\mathrm{C}^{-2}) S_I(0)\,.$$

Modeling the equilibrium current noise by a current source in parallel with a resistor R [17], we may write $S_I(0) \approx 2k_B T/R$. At $T = 1$ K, dephasing time of, e.g., $\tau_{\rm dep} = \Gamma_\varphi^{-1} \approx 1\ \ \mu$s requires $R \approx 1$ kΩ.

The qubit's Rabi time is given by $t_0 = \pi/2\Omega_{\rm ac}$. To achieve $T_1/t_0 \approx 10^3$ (a thousand Rabi oscillations within the decoherence time defined by Gilbert damping), an ac charge current amplitude of 20 μA would be necessary.

We now comment on the upper bound on temperature for the AF to operate in the mono-domain limit. Within the exchange approximation, a thermal magnon mode in the AF with wave number $\boldsymbol{q}$ obeys a linear soundlike dispersion $\omega_{\boldsymbol{q}} = v|\boldsymbol{q}|$, where $v = \sqrt{AL^3/\chi}$ is the magnon velocity and A is the exchange stiffness of the AF. The temperature constraint for mono-domain operation then translates to $T \ll \hbar v\pi/k_B L \equiv T_0$. We then obtain $T_0 \approx J_{\rm AF}(a/L)/k_B$. Estimating again for a cube-shaped $KNiF_3$ with $L = 50$ nm, $J_{\rm AF}/k_B \approx 100$ K and $L/a \approx 125$, we obtain $T_0 > T_+$. So for the relevant operational temperatures of the qubit, the mono-domain assumption is applicable.

To reduce the Joule heating caused by the current in the N, one may reduce J in order to decrease $\bar{j}_c$. However, a decrease in J will also lead to an undesirable decrease in T_+. Alternatively, $\bar{j}_c$ can be reduced with little effect on T_+ by increasing the effective spin Hall angle $\theta_{\rm SH}$; this may be achieved by using materials with strong effective spin Hall angles like topological insulators in place for the N. Achieving qubit operation at small currents is also important in order to minimize decoherence caused by shot noise in the current.

VII. CONCLUSIONS

In this work we introduce the macroscopic spintronic qubit and discuss possible ways to make them interact quantum mechanically. In analogy with the corresponding superconducting devices, including the current-biased Josephson qubits, superconducting quantum annealers, and the superconducting quantum interference device (SQUID) magnetometers, our proposed device could, in principle, be used for preparing macroscopic quantum entanglement, probabilistic information processing, quantum annealing, and quantum-assisted sensing. Our estimation of the relevant physical parameters based on the state-of-the-art technology shows qubit operational temperature that is more than an order of magnitude higher than the existing superconducting qubits, thus opening the possibility of macroscopic quantum information processing at temperatures above the dilution fridge range. While the relaxation time scale $T_1 \approx 10$ ns is relatively short compared to most superconducting devices, antiferromagnets are known to have internal magnetic dynamics in the terahertz range [11]. Further research is needed to demonstrate whether such fast two-qubit time-scale gates could be experimentally achieved with our proposed AF qubits.

VIII. TECHNOLOGICAL CHALLENGES TO SOLID STATE QUANTUM COMPUTING

In general, there are several engineering and technological challenges that have to be overcome in order to pave the way for potential practical relevance of any candidate

solid-state quantum computing architectures [22]. The nature of these obstacles has not yet been fully understood, even for superconducting and silicon-based quantum devices that have been developed for several decades [23,24]. For example, beyond the ratio of the Rabi frequency to decoherence rate, there are other systematic control errors that should be studied and improved, such as the origin of $1/f$ noise, crosstalks, and the limited bandwidth of control electronics, leading to operating frequencies of about 10 GHz for existing superconducting qubits. Quantum hardware needs to be scaled up to a sufficient size to have any chance of being competitive with classical complementary metal-oxide semiconductor (CMOS) technologies that have been exponentially improved for over half of a century. Combining scaling and coherence is the big challenge of quantum systems engineering. This is fundamentally difficult due to the nonseparability of subsystems and the no-cloning theorem, leading to design tradeoffs that are global in nature. It is widely assumed that higher gate fidelities are the only bottleneck for the scalability. This assumption leads to an oversimplification. The two-qubit fidelity is usually characterized in isolation, for optimized sets of parameters, via randomized benchmarking [25]. However, it should be noted that randomized benchmarking only gives a measure of the gate performance in the average case, but the threshold for fault-tolerant quantum computing [26] is established for the worst-case gate performance, which could lead to significantly smaller effective tolerance to errors. Moreover, there are various multiqubit characterizations of the proposed devices that have been traditionally overlooked. These multiqubit performance issues are very important and are different in nature for the near-term digital shallow circuits and quantum annealing processors. There are still several geometrical embedding limitations to achieve a desired computational complexity [27]. These include the degree of parallel operations, denser connectivity graphs, k-local interactions, maximum number of possible couplers, availability of the long-range interactions, and quantum state transfer limitations. There are other fundamental limits to the high-precision tunability, fabrication, and control electronics scalability. These possess several fundamental physical and engineering tradeoffs that are not yet fully understood for any of the major quantum computing proposals.

ACKNOWLEDGMENTS

S.T. would like to thank Pramey Upadhyaya for discussions. This work was supported by FAME (an SRC STARnet center sponsored by MARCO and DARPA).

[1] E. M. Chudnovsky, O. Iglesias, and P. C. E. Stamp, Phys. Rev. B **46**, 5392 (1992); G. Tatara and H. Fukuyama, Phys. Rev. Lett. **72**, 772 (1994); H.-B. Braun and D. Loss, Phys. Rev. B **53**, 3237 (1996); J. Brooke, T. F. Rosenbaum, and G. Aeppli, Nature (London) **413**, 610 (2001).

[2] B. Barbara and E. M. Chudnovsky, Phys. Lett. A **145**, 205 (1990).

[3] E. M. Chudnovsky and L. Gunther, Phys. Rev. Lett. **60**, 661 (1988); D. D. Awschalom, D. P. DiVincenzo, and J. F. Smyth, Science **258**, 414 (1992); S. Gider, D. Awschalom, T. Douglas, S. Mann, and M. Chaparala, *ibid.* **268**, 77 (1995).

[4] A. Chiolero and D. Loss, Phys. Rev. Lett. **80**, 169 (1998); F. Meier and D. Loss, *ibid.* **86**, 5373 (2001); B. Barbara, L. Thomas, F. Lionti, I. Chiorescu, and A. Sulpice, J. Magn. Magn. Mater. **200**, 167 (1999); W. Wernsdorfer and R. Sessoli, Science **284**, 133 (1999).

[5] M. N. Leuenberger and D. Loss, Nature (London) **410**, 789 (2001).

[6] E. B. Sonin, Adv. Phys. **59**, 181 (2010).

[7] A. Schilling and H. Grundmann, Ann. Phys. (NY) **327**, 2301 (2012).

[8] A. Brataas, Y. Tserkovnyak, G. E. W. Bauer, and P. J. Kelly, in *Spin Currents*, edited by S. Maekawa, S. O. Valenzuela, E. Saitoh, and T. Kimura (Oxford University Press, Oxford, 2012), pp. 87–135.

[9] Y. Kajiwara, K. Harii, S. Takahashi, J. Ohe, K. Uchida, M. Mizuguchi, H. Umezawa, H. Kawai, K. Ando, K. Takanashi, S. Maekawa, and E. Saitoh, Nature (London) **464**, 262 (2010); C. W. Sandweg, Y. Kajiwara, A. V. Chumak, A. A. Serga, V. I. Vasyuchka, M. B. Jungfleisch, E. Saitoh, and B. Hillebrands, Phys. Rev. Lett. **106**, 216601 (2011); C. Burrowes, B. Heinrich, B. Kardasz, E. A. Montoya, E. Girt, Y. Sun, Y.-Y. Song, and M. Wu, Appl. Phys. Lett. **100**, 092403 (2012); C. Hahn, G. de Loubens, O. Klein, M. Viret, V. V. Naletov, and J. Ben Youssef, Phys. Rev. B **87**, 174417 (2013).

[10] J. M. Martinis, Quantum Inf. Process. **8**, 81 (2009).

[11] F. Keffer and C. Kittel, Phys. Rev. **85**, 329 (1952); E. V. Gomonay and V. M. Loktev, Low Temp. Phys. **40**, 17 (2014).

[12] T. Kadowaki and H. Nishimori, Phys. Rev. E **58**, 5355 (1998).

[13] S. Takei, B. I. Halperin, A. Yacoby, and Y. Tserkovnyak, Phys. Rev. B **90**, 094408 (2014).

[14] C. Hahn, G. de Loubens, V. V. Naletov, J. B. Youssef, O. Klein, and M. Viret, Europhys. Lett. **108**, 57005 (2014); H. Wang, C. Du, P. C. Hammel, and F. Yang, Phys. Rev. Lett. **113**, 097202 (2014); T. Moriyama, S. Takei, M. Nagata, Y. Yoshimura, N. Matsuzaki, T. Terashima, Y. Tserkovnyak, and T. Ono, Appl. Phys. Lett. **106**, 162406 (2015).

[15] Y. Tserkovnyak and S. A. Bender, Phys. Rev. B **90**, 014428 (2014).

[16] A. Zagoskin and A. Blais, Phys. Can. **63**, 215 (2007).

[17] J. M. Martinis, S. Nam, J. Aumentado, K. M. Lang, and C. Urbina, Phys. Rev. B **67**, 094510 (2003).

[18] L. D. Landau and E. M. Lifshitz, *Statistical Physics*, Part 1, 3rd ed., Course of Theoretical Physics Vol. 5 (Pergamon, Oxford, 1980).

[19] P. Bruno and C. Chappert, *Magnetism and Structure in Systems of Reduced Dimension*, edited by R. F. C. Farrow, B. Dieny, M. Donath, A. Fert, and B. D. Hermsmeier (Springer US, Boston, MA, 1993), pp. 389–399..

[20] L. de Jongh and A. Miedema, Adv. Phys. **23**, 1 (1974).

[21] W. H. Meiklejohn and C. P. Bean, Phys. Rev. **105**, 904 (1957); J. Nogués and I. K. Schuller, J. Magn. Magn. Mater. **192**, 203 (1999).

[22] M. Mohseni, P. Read, H. Neven, S. Boixo, V. Denchev, R. Babbush, A. Fowler, V. Smelyanskiy, and J. Martinis, Nature **543**, 171 (2017).

[23] J. E. Mooij, T. P. Orlando, L. Levitov, Lin Tian, Caspar H. van der Wal, and Seth Lloyd, Science **285**, 1036 (1999).

[24] B. E. Kane, Nature **393**, 133 (1998).

[25] E. Knill, D. Leibfried, R. Reichle, J. Britton, R. B. Blakestad, J. D. Jost, C. Langer, R. Ozeri, S. Seidelin, and D. J. Wineland, Phys. Rev. A **77**, 012307 (2008).

[26] D. Gottesman, Proc. Symp. Appl. Math. **68**, 13 (2009).

[27] S. Boixo, V. N. Smelyanskiy, A. Shabani, S. V. Isakov, M. Dykman, V. S. Denchev, M. H. Amin, A. Yu. Smirnov, M. Mohseni, and H. Neven, Nat. Commun. **7**, 10327 (2016).